Article

The microRNA-200 family regulates pancreatic beta cell survival in type 2 diabetes

BELGARDT, Bengt-Frederik, *et al*.

Abstract

Pancreatic beta cell death is a hallmark of type 1 (T1D) and type 2 (T2D) diabetes, but the molecular mechanisms underlying this aspect of diabetic pathology are poorly understood. Here we report that expression of the microRNA (miR)-200 family is strongly induced in islets of diabetic mice and that beta cell-specific overexpression of miR-200 in mice is sufficient to induce beta cell apoptosis and lethal T2D. Conversely, mir-200 ablation in mice reduces beta cell apoptosis and ameliorates T2D. We show that miR-200 negatively regulates a conserved anti-apoptotic and stress-resistance network that includes the essential beta cell chaperone Dnajc3 (also known as p58IPK) and the caspase inhibitor Xiap. We also observed that mir-200 dosage positively controls activation of the tumor suppressor Trp53 and thereby creates a pro-apoptotic gene-expression signature found in islets of diabetic mice. Consequently, miR-200-induced T2D is suppressed by interfering with the signaling of Trp53 and Bax, a proapoptotic member of the B cell lymphoma 2 protein family. Our results reveal a crucial role for the miR-200 family in beta cell [...]

Reference

BELGARDT, Bengt-Frederik, *et al*. The microRNA-200 family regulates pancreatic beta cell survival in type 2 diabetes. *Nature Medicine*, 2015, vol. 21, no. 6, p. 619-627

DOI : 10.1038/nm.3862
PMID : 25985365

The microRNA-200 family regulates pancreatic beta cell survival in type 2 diabetes

Bengt-Frederik Belgardt[1,2,7], Kashan Ahmed[1,2,7], Martina Spranger[1,2,7], Mathieu Latreille[1,2,6], Remy Denzler[1,2], Nadiia Kondratiuk[1,2], Ferdinand von Meyenn[1,2,6], Felipe Nunez Villena[1,2], Karolin Herrmanns[1,2], Domenico Bosco[3], Julie Kerr-Conte[4], Francois Pattou[4], Thomas Rülicke[5] & Markus Stoffel[1,2]

Pancreatic beta cell death is a hallmark of type 1 (T1D) and type 2 (T2D) diabetes, but the molecular mechanisms underlying this aspect of diabetic pathology are poorly understood. Here we report that expression of the microRNA (miR)-200 family is strongly induced in islets of diabetic mice and that beta cell–specific overexpression of miR-200 in mice is sufficient to induce beta cell apoptosis and lethal T2D. Conversely, *mir-200* ablation in mice reduces beta cell apoptosis and ameliorates T2D. We show that miR-200 negatively regulates a conserved anti-apoptotic and stress-resistance network that includes the essential beta cell chaperone Dnajc3 (also known as p58IPK) and the caspase inhibitor Xiap. We also observed that *mir-200* dosage positively controls activation of the tumor suppressor Trp53 and thereby creates a pro-apoptotic gene-expression signature found in islets of diabetic mice. Consequently, miR-200–induced T2D is suppressed by interfering with the signaling of Trp53 and Bax, a proapoptotic member of the B cell lymphoma 2 protein family. Our results reveal a crucial role for the miR-200 family in beta cell survival and the pathophysiology of diabetes.

Adequate insulin secretion from pancreatic beta cells is necessary to maintain blood glucose levels within a physiological range. During the development of T2D, insulin secretion becomes insufficient to normalize blood glucose levels and eventually beta cell death and reduced beta cell mass ensue in both animal models of and human subjects with overt T2D[1,2]. Apoptosis of beta cells in allogenic islet transplants is also an important factor in the unpredictable durability of these transplants for the treatment of T1D[3]. The molecular underpinnings of diabetic beta cell apoptosis remain poorly understood, although several mechanisms, including inflammation, DNA damage, oxidative and endoplasmatic reticulum stress, have been implicated[2,4–6].

miRs are noncoding RNAs of approximately 22 nucleotides in length that regulate gene expression by inducing degradation and/or translational inhibition of potentially hundreds of target mRNAs[7]. miRs primarily regulate gene expression by binding to the 3′ untranslated region (UTR) of their target mRNA with their 'seed' sequence, which encompasses nucleotides 2–7 of the miR sequence[8]. Our group and others have previously uncovered important metabolic roles for miRs, including in beta cells[9–15].

The miR-200 family consists of five evolutionarily conserved miRs (miR-141, miR-200c, miR-200a, miR-200b and miR-429) and is localized in two polycistronic clusters, *mir-141/200c* and *mir-200a/200b/429* (ref. 16). On the basis of the homology of their seed sequences, miR-200 family members can be subdivided into miR-141/200a (seed AACACUG) and miR-200b/200c/429 (seed AAUACUG), suggesting that they regulate different target genes[17]. Studies in tumor biopsies and cancer cell lines indicate that miR-200 family members may regulate cell differentiation, epithelial-to-mesenchymal transition (EMT) and metastasis[18–20], whereas a recent study linked miR-200b and miR-429 to female fertility and found no signs of EMT when these two *mir-200* family members were ablated *in vivo*[21]. Previous studies have analyzed miR-200 target gene expression in human islets[22] and provided evidence that miR-200b has a role in beta cell apoptosis *in vitro*[23], the latter mediated by Txnip, a protein mediator of the cellular response to oxidative stress. However, the physiological role of the miR-200 family in metabolic regulation and pancreatic beta cell physiology *in vivo* has not been investigated. In this study we examined the miR-200 family in pancreatic beta cells and studied its impact on beta cell survival in response to metabolic stresses. We found that loss of miR-200 function protects against beta cell apoptosis in genetic and pharmacological mouse models that are relevant to human diabetes.

RESULTS

Increased miR-200c levels induce beta cell apoptosis

We examined expression of miR-200 family members in wild-type (WT) mice and found that they are highly expressed in the endocrine pancreas, which mirrors findings in human islets[22,24]

[1]Institute of Molecular Health Sciences, Swiss Federal Institute of Technology, Zurich, Switzerland. [2]Competence Center for Systems Physiology and Metabolic Disease, Swiss Federal Institute of Technology, Zurich, Switzerland. [3]Cell Isolation and Transplantation Center, Department of Surgery, University Hospitals and University of Geneva, Geneva, Switzerland. [4]Université de Lille 2, INSERM, European Genomic Institute for Diabetes, Lille Cedex, France. [5]Institute of Laboratory Animal Science, University of Veterinary Medicine Vienna, Vienna, Austria. [6]Present addresses: Babraham Institute, Cambridge, UK (F.v.M.) and MRC Clinical Sciences Centre, Imperial College London, Hammersmith Hospital, London, UK (M.L.). [7]These authors contributed equally to this work. Correspondence should be addressed to M.S. (stoffel@biol.ethz.ch).

Received 11 February; accepted 15 April; published online 18 May 2015; doi:10.1038/nm.3862

(data not shown). Determination of absolute levels of miR-200 family members by quantitative PCR using synthetic miR standards showed that miR-200c had the highest expression in this location (**Supplementary Fig. 1a**). In normoglycemic obese mice with compensating islet function (high fat diet (HFD)-fed or *ob/ob* mice, both on the C57BL/6 background), miR-200 levels were lower than or similar to those in WT controls (**Fig. 1a**). In *db/db* mice on the C57BLKS/J background (hereafter referred to as *db/db*.BLKS), a mouse model that develops uncontrolled diabetes due to impaired beta cell function and augmented apoptosis[25,26], levels of miR-200 family members were unchanged or lower at 5 weeks of age compared to age-matched WT mice on the same genetic background. However, miR-200 levels in *db/db*.BLKS mice were ~3-fold higher than in WT BLKS mice at 12 weeks of age, at which point this strain of mice is profoundly diabetic (**Fig. 1b**).

To directly test whether T2D-associated overexpression of miR-200 family members in beta cells is causally linked to beta cell apoptosis, we generated transgenic mice expressing *mir-141/200c* under the control of the rat insulin promoter. Three founder lines, hereafter referred to as *Rip141/200c* mice, developed a comparable diabetic phenotype (**Supplementary Fig. 1b**,**c**), and we selected founder E4 for detailed analysis. Levels of miR-141 and miR-200c were ~4- and ~6-fold higher, respectively, in these mice than in WT littermates, an increase similar to the observed ~3-fold level increase of each miR-200 family member in *db/db*.BLKS mice (**Supplementary Fig. 1d**). *Rip141/200c* mice developed severe hyperglycemia, which over time resulted in uncontrolled diabetes and associated symptoms (for example, ketoacidosis and reduced fat mass) (**Fig. 1c**,**d** and **Supplementary Fig. 1e**). Hyperglycemia was due to a drastic decrease in plasma insulin levels, pancreatic insulin content and beta cell mass (>90% loss in mass at 17 weeks of age) (**Fig. 1e**–**g**), without changes in alpha cell mass (**Supplementary Fig. 1f**).

Glucose-stimulated insulin secretion was unaltered in isolated islets of 2-week-old *Rip141/200c* mice and in beta cell lines after overexpression of miR-200c (**Supplementary Fig. 1g** and data not shown). We performed TUNEL staining and found ~6-fold more TUNEL-positive apoptotic cells in islets of *Rip141/200c* mice versus those of WT littermates (**Fig. 1h**). In addition, we excluded other potentially viable mechanisms for reduced beta cell mass, including autoimmune destruction, reduced proliferation and beta-to-alpha cell conversion[27] (**Supplementary Fig. 1h**–**j**).

To address the role of the individual miR-200 family members in the induction of apoptosis, we transfected synthetic mature miRs for all miR-200 family members individually into the mouse beta cell line MIN6. Notably, compared to a control miR, the miRs miR-200b, miR-200c and miR-429 (which share the AAUACUG seed) rapidly induced apoptosis and reduced MIN6 cell counts by 50%, an effect that could be prevented by mutating the seed sequence (**Fig. 1i**,**j**). These data demonstrated that acute and chronic miR-200 overexpression is sufficient to induce beta cell apoptosis and ultimately T2D.

miR-200–null mice have normal glucose tolerance

We next investigated the effects of loss of function of the *miR-200* gene family in pancreatic beta cells and generated mice that are deficient for *mir-141/200c* (hereafter referred to as *141/200c*$^{-/-}$) (**Supplementary Fig. 2a**). No compensation in expression of miR-200a, miR-200b, or miR-429 was observed in *mir-141/200c*–deficient islets (**Supplementary Fig. 2b**). We found that *mir-141/200c*$^{-/-}$ mice were indistinguishable from WT littermates, having

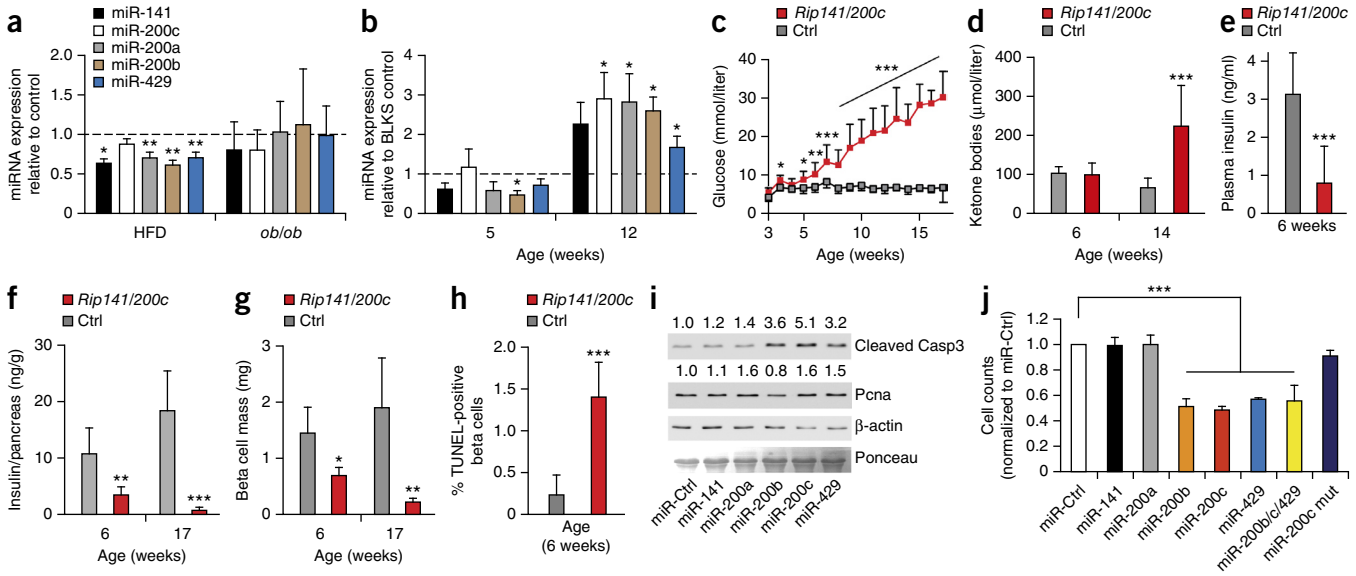

Figure 1 Overexpression of miR-200 causes beta cell death and diabetes. (**a**) Relative expression of miR-141, miR-200a, miR-200b, miR-200c and miR-429 in pancreatic islets of 10-week-old C57BL/6 mice on a normal-chow diet (average miRNA expression, dashed line at 1.0) or a HFD, or those on the *ob/ob* background on a normal-chow diet. Data normalized to normal diet control mice; In **a**,**b**,**d**–**h**, $n = 5$ per genotype. (**b**) Relative expression of the same miRs as in **a** in the pancreatic islets of 5- and 12-week-old *db/db*.BLKS mice. Normalized to BLKS control mice; $P = 0.055$ for miR-141 in *db/db*.BLKS versus WT at 12 weeks. (**c**) Blood glucose levels of randomly fed *Rip141/200c* and WT control (Ctrl) mice. $n = 14$ per genotype. (**d**) Plasma ketone levels of 6- and 14-week-old *Rip141/200c* and Ctrl mice. (**e**) Plasma insulin levels of 6-week-old *Rip141/200c* and Ctrl mice. (**f**) Pancreatic insulin content of *Rip141/200c* and Ctrl mice. (**g**) Pancreatic beta cell mass of *Rip141/200c* and Ctrl mice. (**h**) Quantification of TUNEL-positive pancreatic beta cells in 6-week-old *Rip141/200c* and Ctrl mice. (**i**) Western blot analysis of apoptosis (cleaved Casp3) and mitosis (Pcna) markers after miR mimic transfection in MIN6 cells. Samples from three experiments were pooled for each lane. β-actin and Ponceau, loading controls; numbers, densitometric readouts. (**j**) Automated software-based cell counts of MIN6 cells transfected with miR mimics of miR-141, miR-200a, miR-200b, miR-200c, miR-429, miR-200b/200c/429 combined or miR-200c with mutated seed sequence (mut). $n = 4$, experiments are in quadruplicates. All values are expressed as mean ± s.d. $^{*}P \leq 0.05$, $^{**}P \leq 0.01$, $^{***}P \leq 0.001$; ANOVA with Dunnett's *post hoc* analysis (**j**) or Student's *t*-test (**a**–**h**).

unaltered weight and glucose metabolism when fed either normal chow or HFD (**Supplementary Fig. 2c–j**).

To overcome potential functional compensation by the remaining *mir-200a/200b/429* cluster in *141/200c*$^{-/-}$ mice and to circumvent infertility arising from constitutive miR-429 deficiency[21], we generated *mir-200a/200b/429*–floxed mice (**Supplementary Fig. 3a–c**). By intercrossing these mice with *141/200c*$^{-/-}$ mice and rat insulin promoter Cre (*Rip*-Cre) mice, we obtained mice lacking the entire *mir-200* family in pancreatic beta cells (genotype *mir-141/200c*$^{-/-}$, *Rip*-Cre *mir-200a,200b,429*$^{flox/flox}$; hereafter referred to as double knockout (DKO) mice). Notably, single knockout (KO; either *mir-141/200c*$^{-/-}$ or *Rip*-Cre *mir-200a,200b,429*$^{flox/flox}$) and DKO mice were indistinguishable from littermate controls under unstressed and stressed (HFD) conditions, having normal metabolic parameters, such as glucose metabolism parameters (**Supplementary Fig. 3d–j**), as well as unaltered expression of beta cell identity markers and no consistent upregulation of EMT markers (**Supplementary Table 1**). Our data indicated that, at least in beta cells, loss of all miR-200 family members neither impaired beta cell function nor induced EMT, which is in line with findings in mice with partial *mir-200* ablation[21] or beta cell–specific ablation of the prototypical epithelial marker *Cdh1* (ref. 28).

miR-200 deficiency protects against beta cell apoptosis

Several studies demonstrate that miRs can control vital cellular functions under metabolic stress and thus pathophysiological conditions[29]. To investigate a potential role for the miR-200 family in beta cell demise, we challenged WT, single KO and DKO mice with a low dose of streptozotocin (STZ), an agent known to cause oxidative stress, DNA damage and subsequently beta cell apoptosis and diabetes[2,26]. STZ thus mimics the oxidative and DNA damage found in islets of diabetic subjects[6]. We monitored plasma glucose levels for 15 d after the last of five (once per day) STZ injections. While WT mice developed fasting hyperglycemia, DKO mice exhibited markedly lower plasma glucose levels (**Fig. 2a**). Deficiency of *mir-200a/200b/429* alone was not protective against hyperglycemia. Of note, ablation of *mir-141/200c* or heterozygous *mir-141/200c* deletion combined with homozygous deficiency of *mir-200a/200b/429* in beta cells partially protected animals from STZ-induced hyperglycemia (**Fig. 2a**). This demonstrates that two alleles of *mir-200a/200b/429* can functionally substitute for one *mir-141/200c* allele, which correlates with the approximate 2:1 ratio of absolute expression of the clusters in pancreatic islets (**Supplementary Fig. 1a**).

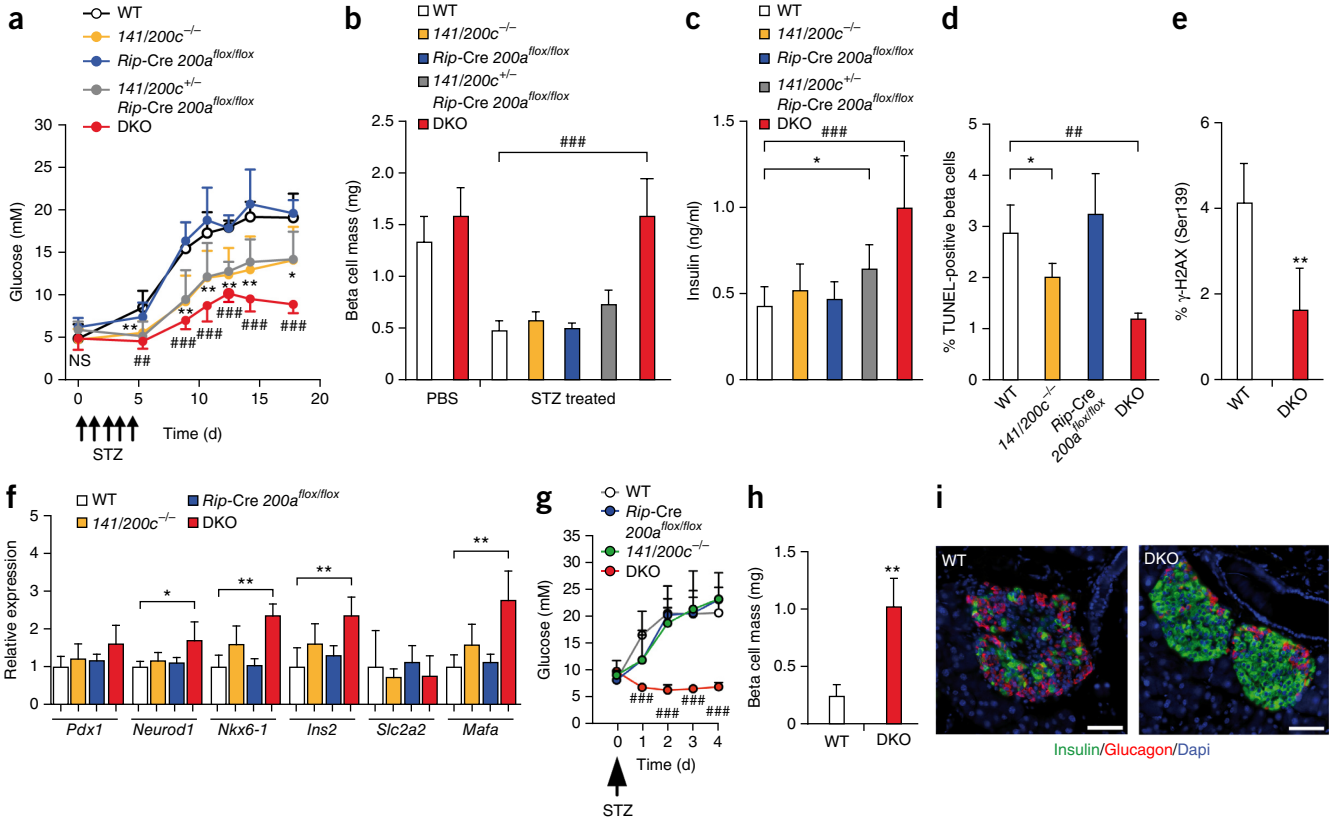

Figure 2 Ablation of *mir-200* protects against STZ-induced beta cell death and diabetes. (**a**) Plasma glucose levels of mice treated with STZ (40 mg/kg) for 5 d. #, *141/200c*$^{+/+}$ versus *141/200c*$^{-/-}$; *, WT versus DKO. $n = 5$ for WT, 13 for *141/200c*$^{-/-}$, 5 for *Rip*-Cre *200a*$^{flox/flox}$, 4 for *141/200c*$^{+/-}$, *Rip*-Cre *200a*$^{flox/flox}$, 5 for DKO. (**b**) Pancreatic beta cell mass 15 d after the last STZ injection or PBS control. $n = 4$. (**c**) Plasma insulin levels of 5 h–fasted mice 15 d after the last STZ injection. *n* values, see **a**. (**d**) Quantification of TUNEL-positive pancreatic beta cells in mice 3 d after the last STZ injection. $n = 5$ for WT, 4 for *141/200c*$^{-/-}$, *Rip*-Cre *200a*$^{flox/flox}$ and DKO. (**e**) Quantification of Ser139-phosphorylated γ-H2AX–positive pancreatic beta cells in mice 3 d after the last STZ injection, $n = 5$ for WT, 4 for DKO. (**f**) qPCR quantification of expression of beta cell identity genes in pancreatic islets from WT, KO and DKO mice treated with a low-dose STZ regimen and analyzed 1 d after the last STZ injection. $n = 4$ per genotype. (**g**) Plasma glucose levels of mice treated with a single STZ injection (150 mg/kg) after 8 weeks of HFD. $n = 11$ for WT, 8 for *141/200c*$^{-/-}$ and DKO, 5 for *Rip*-Cre *200a*$^{flox/flox}$. (**h**) Pancreatic beta cell mass 4 d after a single STZ injection. $n = 4$. (**i**) Representative images ($n = 16$ for both genotypes) of insulin (green), glucagon (red) and DAPI (blue) staining of pancreatic islets in DKO and WT mice 4 d after a single STZ injection. Scale bar, 50 μm. Values are expressed as mean ± s.d. $^{*}P \le 0.05$, $^{**,\#\#}P \le 0.01$, $^{\#\#\#}P \le 0.001$; ANOVA and Tukey's multiple comparison test (**a**–**d**,**f**,**g**) or Student's *t*-test (**e**,**h**). NS, not significant.

Insulin measurements and morphometric analysis of the pancreata revealed that plasma insulin and beta cell mass were ~2-fold and ~3-fold higher, respectively, in DKO mice than in WT mice (**Fig. 2b**,**c**). To investigate if *mir-200* ablation prevented STZ-induced beta cell apoptosis, we performed TUNEL staining 3 d after the last STZ injection. At this time point, WT mice were already severely hyperglycemic, *141/200c*$^{-/-}$ mice had plasma glucose levels that were strongly reduced, and DKO mice were normoglycemic (**Supplementary Fig. 4a**,**b**). Counts of TUNEL-positive beta cells were lower by ~30% in *141/200c*$^{-/-}$ and ~60% in DKO mice, as compared to WT and *Rip*-Cre *mir-200a/200b/429*$^{flox/flox}$ animals (**Fig. 2d**). Furthermore, histone γ-H2AX, which is phosphorylated in response to oxidative and DNA damage in islets of diabetic *db*/*db*.BLKS mice[30], was ~50% less phosphorylated (**Fig. 2e** and **Supplementary Fig. 4c**), inflammatory markers were unchanged (**Supplementary Fig. 4d**), and transcript levels of oxidative defense genes such as those encoding the glutathione peroxidases (*Gpx1*, *Gpx3*, and *Gpx4*) and catalase (*Cat*) were augmented (**Supplementary Fig. 4e**) in islets from STZ-treated DKO mice versus those from STZ-treated WT mice. Proliferation of beta cells was similar in WT and DKO mice at day 8, indicating that protection of beta cells from apoptosis is the initial event in *mir-200*–deficient mice. At day 20, more beta cell proliferation was present in STZ-treated DKO compared to STZ-treated WT mice (**Supplementary Fig. 4f**), suggestive of additional late-acting protective events. Expression of beta cell identity markers, which is decreased by STZ treatment[31], remained high in pancreatic islets from DKO as compared to control animals, which may contribute to improved glycemic control (**Fig. 2f**).

In a second model of obesity-enhanced beta cell destruction and diabetes, we challenged HFD-induced obese control and DKO mice with a single high-dose (150 mg/kg) administration of STZ (ref. 2). While control animals suffered from massive loss of beta cell mass and diabetes, DKO mice were completely protected against hyperglycemia and beta cell loss (**Fig. 2g–i** and **Supplementary Fig. 4g–i**).

We next investigated whether loss of miR-200 function is also protective in Akita mice, a well-characterized genetic T2D model in which a spontaneous mutation in the insulin 2 (*Ins2*) gene causes chronic insulin misfolding, endoplasmatic reticulum stress, pro-apoptotic gene expression and subsequently beta cell apoptosis and diabetes[2,5]. Much as in the STZ models, we observed ameliorated hyperglycemia, improved plasma insulin levels, augmented beta cell mass (**Fig. 3a–d**), higher levels of anti-apoptotic miR-200 targets and lower expression of ER stress markers, including *Hspa5* and *Ddit3*, when miR-200 expression was absent or reduced in these mice (**Supplementary Fig. 5a** and **Fig. 3e**). In summary, ablation of the *miR-200* family inhibited beta cell apoptosis, prevented loss of beta cell mass, improved plasma insulin levels and strongly ameliorated hyperglycemia in multiple diabetic mouse models with hyperactive pathophysiological stress pathways known to be relevant in human diabetes.

miR-200 regulates anti-apoptotic target genes

As mammalian miRs mostly act by destabilizing target mRNAs[32], we generated transcriptome-wide expression profiles from *Rip141/200c* islets, DKO islets, MIN6 cells with adenoviral overexpression of miR-141/200c and controls (islets from WT littermates and Ad-GFP–expressing MIN6 cells) using Affymetrix arrays and RNA-seq. We confirmed by bioinformatic analyses that overexpression of miR-141/200c in these settings was specific to the miR-141/200c seed sequence and did not affect target gene populations of other relevant miRs, such as miR-7 (ref. 10) (**Supplementary Fig. 5b–d**).

We next sought to define the mRNA target(s) of the miR-200 family with prosurvival properties in beta cells. To this end, we set up a series of *in vitro* and *ex vivo* experiments in which all candidate mRNAs were assessed. We tested potential targets carrying at least one miR-200c heptamer miR response element (MRE) to determine whether they were decreased in the overexpression or increased in the loss-of-function profiles using expression level and 1.2-fold change cut-offs. From this selection, we first concentrated on candidate targets that were previously associated with beta cell function, apoptosis or ER stress or were linked to T2D risk in genome-wide association studies. In addition we examined candidate genes independent of any previous association with beta cell function or apoptosis that were regulated in at least two of the transcriptome data sets.

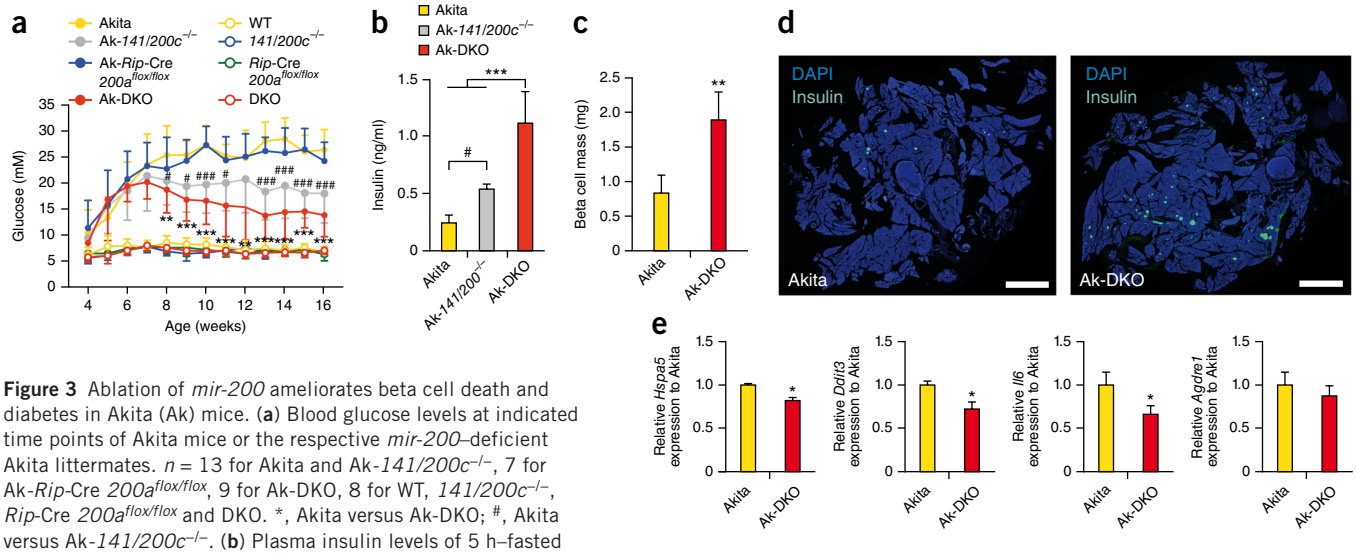

Figure 3 Ablation of *mir-200* ameliorates beta cell death and diabetes in Akita (Ak) mice. (**a**) Blood glucose levels at indicated time points of Akita mice or the respective *mir-200*–deficient Akita littermates. $n = 13$ for Akita and Ak-*141/200c*$^{-/-}$, 7 for Ak-*Rip*-Cre *200a*$^{flox/flox}$, 9 for Ak-DKO, 8 for WT, *141/200c*$^{-/-}$, *Rip*-Cre *200a*$^{flox/flox}$ and DKO. *, Akita versus Ak-DKO; #, Akita versus Ak-*141/200c*$^{-/-}$. (**b**) Plasma insulin levels of 5 h–fasted mice of the indicated genotype at 16 weeks of age, $n = 7$ for Akita and Ak-DKO, 4 for Ak-*141/200c*$^{-/-}$. (**c**) Pancreatic beta cell mass of mice of the indicated genotype at 16 weeks of age. $n = 5$. (**d**) Representative images ($n = 25$ for Akita, 23 for Ak-DKO) of a pancreatic section from Akita and Ak-DKO mice at 16 weeks of age, stained for insulin (green) and DAPI (blue). Scale bars, 2 mm. (**e**) Relative expression of ER stress and inflammatory markers in islets from Akita and Ak-DKO mice. $n = 4$. Values are expressed as mean ± s.d. $^{*,\#}P \le 0.05$, $^{**}P \le 0.01$, $^{***,\#\#\#}P \le 0.001$; ANOVA and Tukey's multiple comparison test (**a**,**b**) or Student's *t*-test (**c**,**e**).

The criteria above were fulfilled by four mRNAs, encoded by the following genes: the DnaJ (Hsp40) homolog, subfamily C, member 3 gene (*Dnajc3*), juxtaposed with the JAZF zinc finger 1 gene (*Jazf1*), the prosurvival ribosomal protein S6 kinase, polypeptide 1 gene (*Rps6kb1*, also known as p70s6K), and the X-linked inhibitor of apoptosis gene (*Xiap*). Dnajc3 (also known as p58IPK) is an essential beta cell chaperone, as *Dnajc3*-deficient mice exhibit spontaneous beta cell apoptosis and develop T2D[33]. *JAZF1* harbors a susceptibility locus for T2D in its first intron and shows decreased expression in the beta cells of humans with T2D, although its functional role in beta cells has not yet been addressed[34,35]. Rps6kb1 is a kinase downstream of mTOR and other growth factor signaling pathways and known to inactivate the pro-apoptotic protein Bad[36,37]. XIAP binds to and inhibits several caspases including CASP3, and overexpression of XIAP is protective against beta cell stress in both mice and humans, whereas loss of *Xiap* in mice does not cause an identifiable abnormal phenotype under unstressed conditions[38–40].

Alignment of 3′ UTRs of all four genes revealed evolutionarily conserved MREs for miR-200c, indicating that these sequences mediate a basic regulatory function (**Supplementary Fig. 5e**). We first confirmed regulation of these genes by qPCR (or by immunoblotting if specific commercial antibodies were available) in an independent set of *Rip141/200c* islets as well as upon overexpression of miR-200 in mouse beta cells and in human cell line HEK 293 (**Fig. 4a–c**). Additionally, we determined that expression of miR-200 targets was higher in DKO than in WT islets (**Supplementary Fig. 5f**). We also confirmed target regulation in the Akita mouse model and in human islets when *mir-200* was genetically deleted or silenced with antagomirs (anti-miRs), respectively (**Supplementary Figs. 5a** and **6**). Furthermore, acute miR-200 overexpression in INS-1E cells also affected the activity of Eif2a, an established downstream effector of Dnajc3 (ref. 41) (**Fig. 4d**). Next we used luciferase reporter assays based on luciferase constructs harboring WT or mutated miR-200c MREs sequences in the 3′ UTR to confirm that all four genes were direct targets of miR-200c, but not of miR-141 (**Fig. 4e,f**).

As a third step, we transfected two independent siRNAs against all four target genes into beta cell lines and determined their effect on apoptosis. Knockdown of each transcript except that of *Xiap* induced apoptosis, as determined by cleavage of Casp3, and hence reduced beta cell counts by up to 40% 72 h after transfection (**Fig. 4g,h**).

We also investigated if miR-200 regulation of *Zeb1*, a previously described miR-200 target, might affect the differentiation state of beta cells[23]. Overexpression of miR-200 or reduced miR-200 levels (*mir-141/200c*$^{-/-}$) did not change the expression of *Zeb1* and its downstream targets (**Supplementary Table 1**). Only DKO mice exhibited higher *Zeb1* levels and regulation of a restricted subset of EMT markers, including *Cdh1* (**Supplementary Table 1**), but without any alteration of islet morphology, beta cell function or expression of beta cell identity genes (**Supplementary Fig. 3d–f**).

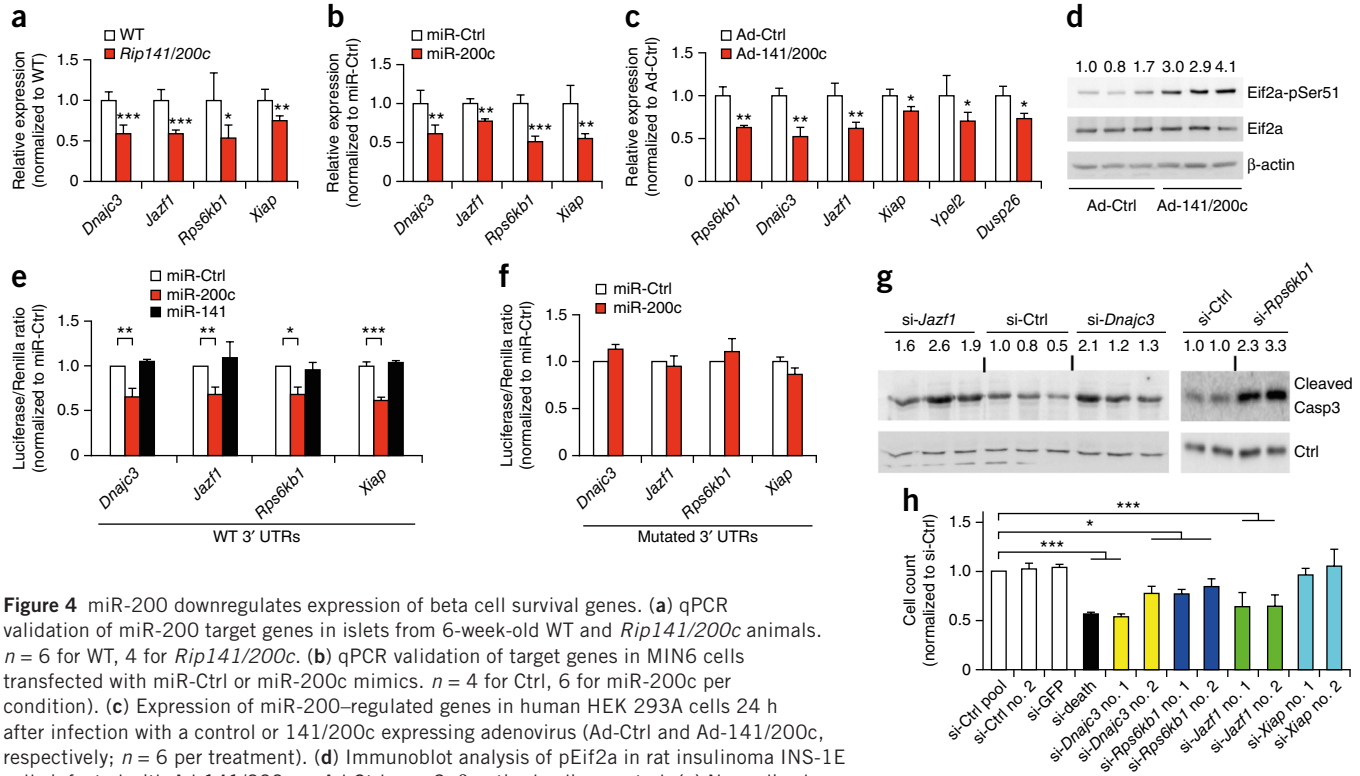

Figure 4 miR-200 downregulates expression of beta cell survival genes. (**a**) qPCR validation of miR-200 target genes in islets from 6-week-old WT and *Rip141/200c* animals. $n = 6$ for WT, 4 for *Rip141/200c*. (**b**) qPCR validation of target genes in MIN6 cells transfected with miR-Ctrl or miR-200c mimics. $n = 4$ for Ctrl, 6 for miR-200c per condition). (**c**) Expression of miR-200–regulated genes in human HEK 293A cells 24 h after infection with a control or 141/200c expressing adenovirus (Ad-Ctrl and Ad-141/200c, respectively; $n = 6$ per treatment). (**d**) Immunoblot analysis of pEif2a in rat insulinoma INS-1E cells infected with Ad-141/200c or Ad-Ctrl. $n = 3$. β-actin, loading control. (**e**) Normalized luciferase activity assays for WT 3′ UTRs of *Dnajc3*, *Jazf1*, *Rps6kb1* or *Xiap* after miR-Ctrl, miR-200c or miR-141 treatment. $n = 3$. (**f**) Normalized luciferase activity assays for 3′ UTRs of *Dnajc3*, *Jazf1*, *Rps6kb1* or *Xiap* with mutated miR-200b/200c/429 MREs after miR-Ctrl or miR-200c treatment. $n = 3$. (**g**) Immunoblot analysis of cleaved Casp3 in MIN6 cells after transfection with pooled siRNAs targeting *Jazf1*, *Dnajc3*, *Rps6kb1* or with a control siRNA pool. $n = 3$ per condition. Loading controls (Ctrl), β-actin (left) and tubulin (right). Densitometric quantification of cleaved Casp3 as depicted above each lane was normalized to Ctrl bands. (**h**) Automated software-based cell counts of MIN6 cells treated with three different control siRNAs or two siRNAs each targeting *Dnajc3*, *Jazf1*, *Rps6kb1* or *Xiap*. A commercially available death-inducing siRNA (si-death) was used as a positive control. Si-GFP was also used as a control. $n = 3$ independent experiments each performed in quadruplicates. Values are expressed as mean ± s.d. $^*P \leq 0.05$, $^{**}P \leq 0.01$, $^{***}P \leq 0.001$; ANOVA with Dunnett's *post hoc* analysis (**e**,**h**) or Student's *t*-test (**a**–**c**,**f**).

In addition to the genes described above, expression of *Dusp26*, which encodes dual specificity phosphatase 26, a protein that has been linked to prosurvival signaling[42], was also strongly reduced (~60%) in *Rip141/200c* mice and higher in islets of both unstressed and STZ-treated DKO animals (**Fig. 5a**,**b**), which was replicated by acute miR-200c manipulation in mouse and human cells (**Figs. 4c** and **5c**). To define the role of Dusp26 in beta cells, we silenced *Dusp26* by RNA interference, which reduced beta cell counts and induced apoptosis *in vitro* (**Fig. 5d**,**e**). *Dusp26* silencing also induced phosphorylation of the prototypical regulator of apoptosis, Trp53, at Ser15 (Trp53-pSer15)[43] (**Fig. 5e**). This post-translational modification is used as a marker for Trp53 activity[43]. Surprisingly, *Dusp26* harbors no functional miR-200 MRE, indicating that miR-200 regulated one or more intermediate direct target genes to affect *Dusp26* expression. To identify these intermediate target genes, we performed a second screen and found seven genes that were directly targeted by miR-200c and were necessary for full *Dusp26* expression (**Supplementary Fig. 7a**,**b**). Among them was *Ypel2*, a potential oncogene of unknown function, which has previously been associated with pancreatic and breast cancer[44]. *Ypel2* harbors a conserved and functional miR-200c binding site in its 3′ UTR (**Supplementary Fig. 5e**), as confirmed in luciferase reporter assays (**Supplementary Fig. 7c**,**d**). *Ypel2* levels were lower in *Rip141/200c* islets and upon transfection of miR-200c into INS-1E cells *in vitro* (**Supplementary Fig. 7e**,**f**). Conversely, expression of *Ypel2* was higher in islets lacking miR-200 (**Supplementary Fig. 5f**). Knockdown of *Ypel2* reduced *Dusp26* expression (**Supplementary Fig. 7g**), stimulated phosphorylation of Trp53-pSer15 (**Fig. 5f**), induced Trp53 target gene expression (**Fig. 5g**), activated cleavage of Casp3 (**Supplementary Fig. 7h**) and reduced beta cell counts (**Supplementary Fig. 7i**). We concluded that *Dusp26* expression is regulated indirectly by miR-200c through several direct targets including *Ypel2*. Together, these results indicate that miR-200c regulates prosurvival, anti-apoptosis and ER-stress pathways in parallel through several direct target genes in pancreatic beta cells.

miR-200 regulates the Trp53 network

We next used an independent and unbiased bioinformatic approach to identify the gene networks that are responsible for miR-200–induced beta cell apoptosis. This analysis, which compared miR-200–regulated

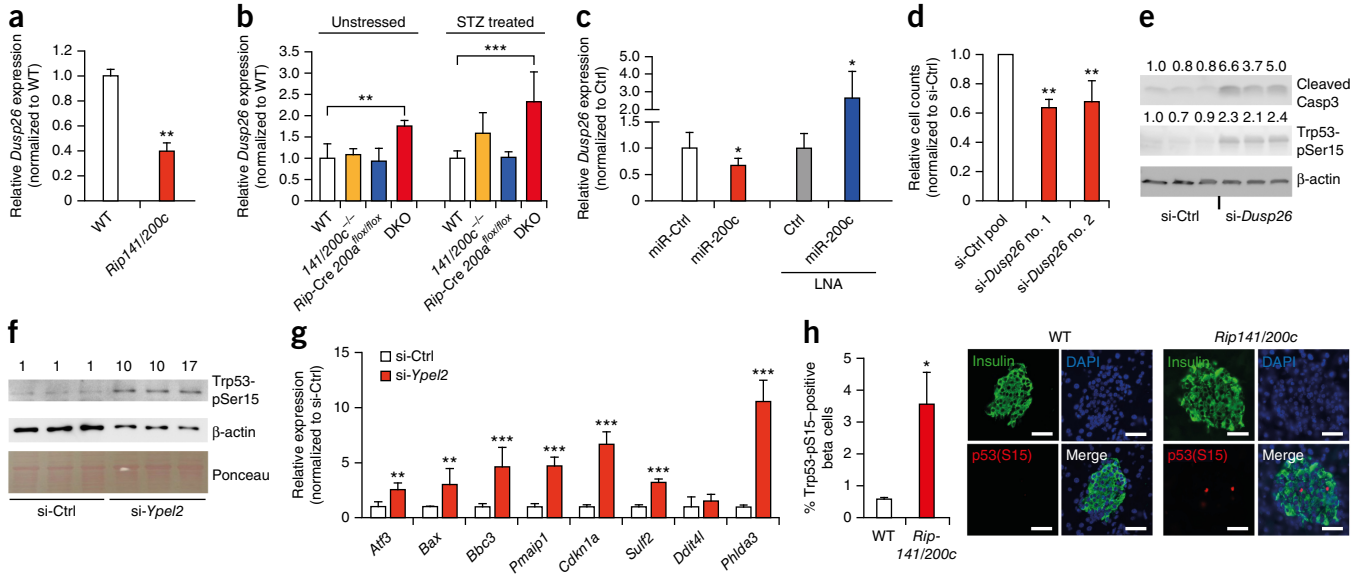

Figure 5 miR-200–mediated regulation of Trp53 activity. (**a**) qPCR quantification of *Dusp26* expression in pancreatic islets of 6-week-old *Rip141/200c* and control littermates. $n = 6$ for WT, 4 for *Rip141/200c*. (**b**) qPCR quantification of *Dusp26* expression in islets from WT, single KO and DKO littermates that were untreated (unstressed) or treated with low-dose STZ for 5 d. $n = 4$ per genotype. (**c**) *Dusp26* expression in MIN6 cells after transfection with miR-200 mimics or locked nucleic acids (LNA) inhibitors and controls. $n = 3$. (**d**) Automated software-based cell counts of INS-1E cells treated with the siRNA control pool or two unique siRNAs each targeting *Dusp26*. $n = 4$ per treatment. (**e**) Immunoblot analysis of Trp53-pSer15 and cleaved Casp3 as a marker for Trp53 activation and apoptosis, respectively, after si-*Dusp26* treatment in INS-1E cells. Cleaved Casp3 and Trp53-pSer15 signals were quantified by densitometer in comparison to β-actin and are depicted above each lane ($n = 3$ per treatment). (**f**) Immunoblot analysis of Ins1 cells transfected with siRNA targeting *Ypel2* using anti-Trp53-pSer15 antibodies. $n = 3$ per condition. Numbers above each lane indicate densitometric quantification of Trp53-pSer15 normalized to β-actin. Ponceau, additional loading control. (**g**) Expression of Trp53 targets in INS-1E cells upon knockdown of *Ypel2* by RNAi. $n = 6$ per condition. (**h**) Quantification (left) and representative images (right; $n = 20$ for each genotype) of Trp53-pSer15 staining (red) in beta cells from *Rip141/200c* and WT mice. $n = 3$ per genotype. Here and in **i**, sections were also stained for insulin (green) and DAPI (blue). Scale bars, 25 μm. (**i**) Quantification (left) and representative images (right; $n = 39$ for WT, 38 for DKO) of Trp53-pSer15 staining (red) in beta cells from DKO and WT mice 3 d after the last STZ injection ($n = 5$ for WT, 4 for DKO). Scale bars, 50 μm. (**j**) Immunoblot analysis for Trp53-pSer15, Trp53 and γ-tubulin in WT and DKO mice treated with STZ as in **i**. Numbers, densitometric quantification of Trp53-pSer15 normalized to γ-tubulin. All values are expressed as mean ± s.d. $^*P \le 0.05$, $^{**}P \le 0.01$, $^{***}P \le 0.001$; ANOVA and Tukey's multiple comparison test (**b**), Dunnett's *post hoc* analysis (**d**), or Student's *t*-test (**a**,**c**,**g**–**i**).

genes with published targets of transcription factors, pointed to the tumor suppressor Trp53 network as the most significantly regulated hub for upstream regulators (Ad-141/200c–expressing MIN6 cells, $P = 2 \times 10^{-10}$; *Rip141/200c* islets, $P = 6 \times 10^{-34}$, **Supplementary Fig. 8a**). To confirm that Trp53 activity correlates with apoptosis in pancreatic islets of *Rip141/200c* and STZ-treated DKO mice, we quantified Trp53-pSer15 by immunoblotting and immunohistochemistry. The number of Trp53-pSer15–positive beta cells was ~3-fold higher in *Rip141/200c* mice, whereas DKO mice exhibited a 70–80% reduction in Trp53-pSer15–positive beta cells compared to STZ-treated controls (**Fig. 5h,i**), which was confirmed by measuring protein levels by immunoblot analysis (**Fig. 5j** and **Supplementary Fig. 8b**). Furthermore, acute adenoviral overexpression of miR-200 also potently induced Trp53-pSer15 levels *in vitro* (**Supplementary Fig. 8c**).

Overexpression of miR-200c induced Trp53-regulated transcripts of *Bax*, *Bbc3* (encoding Puma), *Pmaip1* (encoding Noxa) and other validated Trp53 targets, including *Cdkn1a* (encoding P21), *Ddit4l* (encoding DNA-damage-inducible transcript 4-like), *Sulf2* (encoding sulfatase 2) and *Phlda3* (encoding pleckstrin homology-like domain, family A, member 3), in islets of *Rip141/200c*, as compared to that in WT mice (**Fig. 6a**). This pro-apoptotic expression pattern was limited to the miR-200b/200c/429 seed sequence (**Supplementary Fig. 8d**). Previously, strong induction of several Trp53 target genes after STZ treatment was reported[31]. Among those genes, *Cdkn1a*, *Ddit4l*, *Sulf2* and *Phlda3* were reduced in islets from STZ-treated DKO mice (**Supplementary Fig. 8e**). Furthermore, inhibition of miR-200c in primary human islets by anti-miRs was sufficient to blunt expression of pro-apoptotic genes induced by diabetes-associated cytokine treatment (**Supplementary Fig. 9**)

Treatment with Nutlin-3 (N3), a pharmacological activator of Trp53, confirmed that these genes are under the transcriptional control of Trp3 in beta cells, and N3 treatment induced apoptosis and reduced MIN6 cell counts (data not shown). We observed elevated expression of *Atf3* (encoding activating transcription factor 3), *Bax*, *Bbc3*, *Pmaip1* and *Phlda3* in islets from diabetic *db/db*.BLKS versus WT mice on a BLKS background at the same time as miR-200 induction. This effect was absent or milder in younger, still prediabetic *db/db* animals, in which miR-200 expression was low (**Fig. 6b**). Importantly, *Atf3*, *Bax* and *Bbc3* are causally linked to mouse beta cell death and are associated with human beta cell apoptosis and diabetes[45–47]. The role of Phlda3 in beta cells has not been directly studied[48]. A previous report demonstrates that Phlda3 prevents activation of the prosurvival kinase Akt, which is also involved in preventing beta cell death[48,49]. Notably, we found that overexpression of human Phlda3 was sufficient to induce apoptosis and reduce beta cell counts *in vitro* (data not shown).

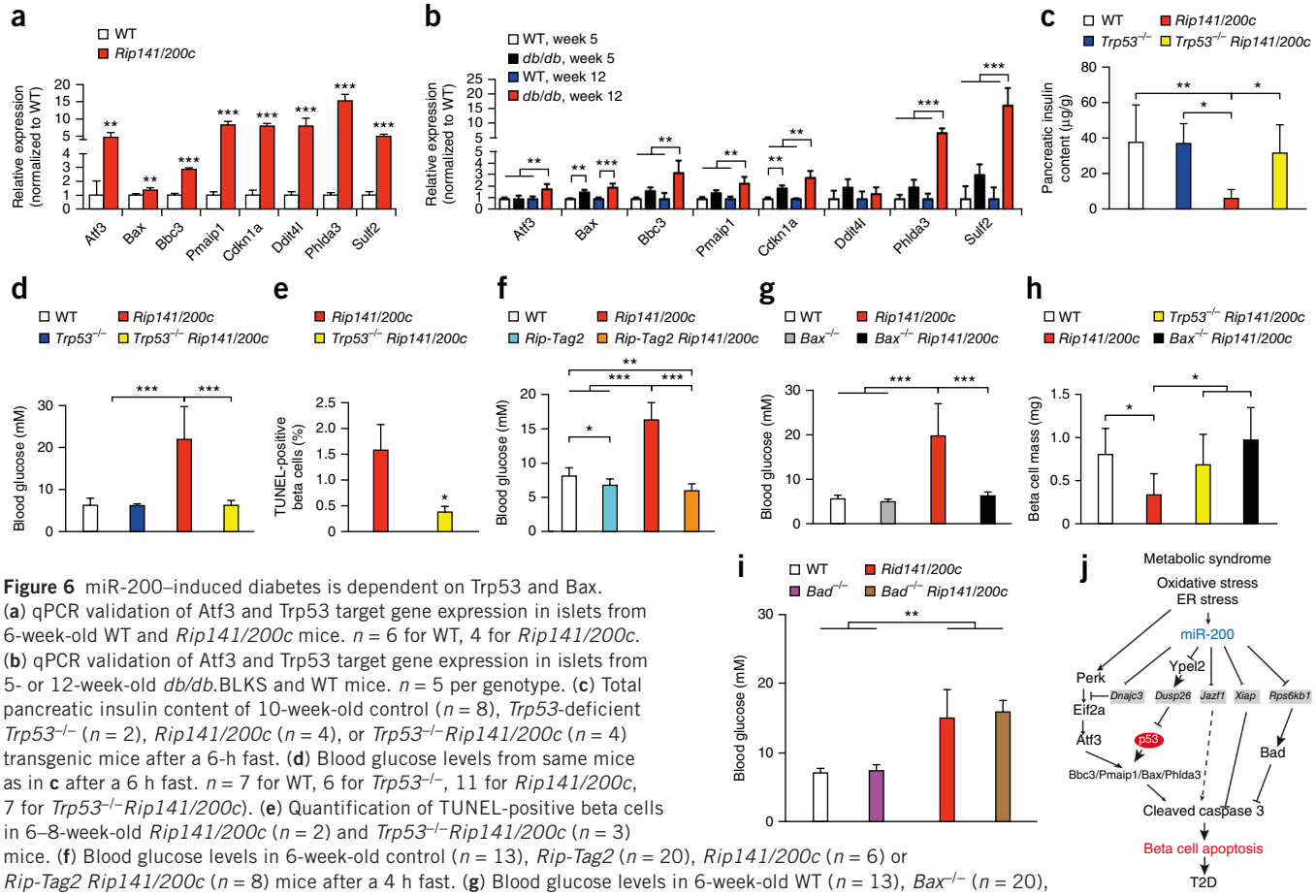

Figure 6 miR-200–induced diabetes is dependent on Trp53 and Bax. (**a**) qPCR validation of Atf3 and Trp53 target gene expression in islets from 6-week-old WT and *Rip141/200c* mice. $n = 6$ for WT, 4 for *Rip141/200c*. (**b**) qPCR validation of Atf3 and Trp53 target gene expression in islets from 5- or 12-week-old *db/db*.BLKS and WT mice. $n = 5$ per genotype. (**c**) Total pancreatic insulin content of 10-week-old control ($n = 8$), *Trp53*-deficient *Trp53*$^{-/-}$ ($n = 2$), *Rip141/200c* ($n = 4$), or *Trp53*$^{-/-}$*Rip141/200c* ($n = 4$) transgenic mice after a 6-h fast. (**d**) Blood glucose levels from same mice as in **c** after a 6 h fast. $n = 7$ for WT, 6 for *Trp53*$^{-/-}$, 11 for *Rip141/200c*, 7 for *Trp53*$^{-/-}$*Rip141/200c*). (**e**) Quantification of TUNEL-positive beta cells in 6–8-week-old *Rip141/200c* ($n = 2$) and *Trp53*$^{-/-}$*Rip141/200c* ($n = 3$) mice. (**f**) Blood glucose levels in 6-week-old control ($n = 13$), *Rip-Tag2* ($n = 20$), *Rip141/200c* ($n = 6$) or *Rip-Tag2 Rip141/200c* ($n = 8$) mice after a 4 h fast. (**g**) Blood glucose levels in 6-week-old WT ($n = 13$), *Bax*$^{-/-}$ ($n = 20$), *Rip141/200c* ($n = 6$) or *Bax*$^{-/-}$*Rip141/200c* ($n = 8$) mice after a 4 h fast. (**h**) Beta cell mass of 10-week-old control ($n = 3$), *Rip141/200c* ($n = 11$), *Trp53*$^{-/-}$*Rip141/200c* ($n = 5$) or *Bax*$^{-/-}$*Rip141/200c* ($n = 3$) mice. (**i**) Blood glucose levels in 10-week-old control ($n = 11$), *Bad*$^{-/-}$ ($n = 4$), *Rip141/200c* ($n = 13$) or *Bad*$^{-/-}$*Rip141/200c* ($n = 4$) mice after a 4 h fast. (**j**) Schematic illustration of miR-200–regulated pathways leading to apoptosis in pancreatic beta cells. All data are expressed as mean ± s.d. $^{*}P \le 0.05$, $^{**}P \le 0.01$, $^{***}P \le 0.001$; ANOVA and Tukey's multiple comparison test (**b**–**d**,**f**,**g**,**i**), Fisher's LSD test (**h**) or Student's *t*-test (**a**,**e**).

Ablation of *Trp53* and *Bax* alleviates miR-200–induced apoptosis

To directly test whether these pro-apoptotic genes were induced in a strictly Trp53-dependent manner, we treated WT or *Trp53*-deficient islets with STZ *ex vivo*. STZ strongly induced expression of *Atf3* mRNA as well as all Trp53 target genes tested in control islets (**Supplementary Fig. 10a**). In contrast, expression of *Atf3*, but not of any of the seven Trp53 target genes tested, was profoundly upregulated in STZ-treated *Trp53*$^{-/-}$ islets (**Supplementary Fig. 10a**).

To directly address whether miR-200c–induced diabetes can be rescued by genetic *Trp53* deficiency or inhibition, we bred *Rip141/200c* mice with either *Trp53*$^{-/-}$ mice or *Rip-Tag2* mice, which specifically overexpress the Trp53-inhibiting SV40 T antigen in beta cells only[50]. In both settings, the ability of miR-200c to induce its pro-apoptotic gene suite was blunted, and it failed to cause T2D (**Fig. 6c–f** and **Supplementary Fig. 10b**,**c**). Knockout of the pro-apoptotic B cell lymphoma 2family member *Bax*, which is crucial for Trp53-induced apoptosis[51], similarly protected against pancreatic beta cell loss and prevented T2D in *Rip141/200c* mice (**Fig. 6g**,**h** and **Supplementary Fig. 10d**). The extreme glucose intolerance of *Rip141/200c* mice was ameliorated but not completely rescued when *Trp53* or *Bax* was ablated, indicating that additional (Trp53- and Bax-independent) miR-200–induced deleterious pathways exist (**Supplementary Fig. 10e**). Ablation of the gene encoding the pro-apoptotic protein Bad, which is related to Bax and inactivated by Rps6kb1 (refs. 36,37), was insufficient to prevent diabetes, underlining the specificity and redundancy of the miR-200 cell death pathways (**Fig. 6i–j**).

DISCUSSION

The results presented here underscore the cell type–, cluster- and seed-specific function of the miR-200 family in pancreatic beta cell survival *in vivo*. Our data demonstrate that miR-200b, miR-200c and miR-429, which share the same seed sequence, are the principal regulators of beta cell apoptosis in pathophysiological models of T2D. Ablation of *mir-200c* (but not *mir-200b* and *mir-429*, which contain identical seed sequences but are expressed at lower copy numbers) partially protects against beta cell demise in response to oxidative and ER stress, while combined ablation of both clusters of the *mir-200* family confers the strongest protection against beta cell apoptosis. Therefore, selective pharmacological targeting[52,53] of the miR-200b/200c/429 seed sequence may be efficacious for protecting beta cells from diabetogenic insults. Importantly, a total loss of *mir-200* expression does not result in EMT or cellular dedifferentiation, at least in beta cells (this remains to be tested in other epithelial cell types).

We find that expression of both *mir-200* clusters is elevated under diabetic conditions. While several transcription factors, including Trp53 and Txnip, can regulate miR-200 expression[23,54], neither acute induction of ER stress, oxidative stress, Trp53 activation nor *Trp53* ablation altered miR-200 expression in mouse islets (data not shown), indicating that regulation of miR-200 expression is complex and cell-type specific.

Ablation of *mir-200* protects against both oxidative and DNA damage stress (STZ model) and ER stress (Akita model) *in vivo*, which are known to contribute to beta cell death in rodent and human diabetes[4–6]. Future studies need to clarify whether miR-200 also mitigates cellular stresses *per se*. There is clear evidence that the miR-200 family (and probably all miRs) simultaneously target multiple genes and molecular pathways to affect cellular fate[7,20], and here we define a network of prosurvival and anti-apoptotic genes that are targeted by the miR-200 family. miR-200 targets *Dnajc3*, which encodes an established and crucial chaperone in beta cells, and lower Dnajc3 levels may partially explain the higher *Atf3* mRNA levels detected upon miR-200 overexpression[33,55]. Loss of *mir-200* also promotes survival by de-repressing *Xiap*, a potent inhibitor of caspase activation. In this regard, overexpression of XIAP protects human beta cells against apoptosis[38]. Reduced miR-200 activity may also engage other anti-stress and/or prosurvival pathways, for example through *JAZF1*, a T2D susceptibility locus[34] whose targets and precise mode of action remain to be established. Functional analysis of genetic models with mutations in miR-200 response elements (including the target *Zeb1*, which contains five miR-200b/200c/429 seed matches in its 3′ UTR[16,18]) will help to delineate the relative importance of each target gene.

Our data further indicate that miR-200 modulates the activity of Trp53 through regulation of several direct target genes, most notably *Ypel2*, which is necessary for full expression of *Dusp26*, a phosphatase that in turn controls TRP53 (ref. 42). We therefore propose that during pathophysiological stress conditions *mir-200* dosage impacts on several parallel and conserved apoptotic pathways, including ATF3- and TRP53-dependent networks[30,45–47,56]. These findings may not only be relevant in the context of beta cell apoptosis and diabetes. Loss of *Trp53* and altered expression of *mir-200* are commonly detected in tumorigenesis, and several direct miR-200 targets and executor proteins verified in this study have been linked to tumor formation[44,57,58]. Further analysis of their interaction will be informative in regard to endocrine tumor development (for example, insulinoma) and other physiological processes such as postpartum-associated islet remodeling.

In summary, we demonstrate that the miR-200 family is a crucial endogenous regulator of T2D-associated beta cell apoptosis through pleiotropic stress-resistance and prosurvival pathways (**Fig. 6j**), and this finding further highlights the crucial influence of miRs on beta cell function[9–12]. Inhibiting miR-200 activity may be a potential pharmacological strategy to promote beta cell survival.

METHODS

Methods and any associated references are available in the online version of the paper.

Accession codes. Gene Expression Omnibus: Coordinates have been deposited with accession codes GSE58487 (MIN6 cells) and GSE58488 (islets).

Note: Any Supplementary Information and Source Data files are available in the online version of the paper.

ACKNOWLEDGMENTS

We wish to thank B. Kaps and R. Kubsch for excellent technical and animal husbandry assistance. We thank the Functional Genomics Center Zurich and the Light Microscopy and Screening Center Zurich for support, and N. Danial (Dana Farber Cancer Institute, Boston, USA), D. Hanahan (Swiss Institute for Experimental Cancer Research, Lausanne, Switzerland) and P. Herrera (University of Geneva, Switzerland) for sharing *Bad*$^{-/-}$, *Rip-Tag2* and *Rip*-Cre mice, respectively. This work was supported by European Molecular Biology Organization Long-Term Fellowships (to B.-F.B. and K.A.), the Austrian Genome Research Programme GEN-AU II and III (Austromouse) (to T.R.) and the European Genomic Institute for Diabetes (ANR-10-LABX-46 to F.P.) and in part sponsored by a Juvenile Diabetes Research Foundation (JDRF) Scholar award, European Research Council grant 'Metabolomirs', the Starr Foundation International and the Swiss National Science Foundation, and the National Center of Competence in Research on RNA Biology and Disease (all to M.S.). Human islets for research were provided thanks to the European Consortium for Islet Transplantation funded by the JDRF (31-2012-783 to F.P.).

AUTHOR CONTRIBUTIONS

B.-F.B. and K.A. performed most of the experiments, analyzed and interpreted data and wrote the manuscript; K.A. generated conditional *miR-200a*$^{flox/flox}$ mice;

M.S. generated *Rip141/200c* and *mir-141/200c*$^{-/-}$ animals and performed the initial characterizations; M.L. generated miR expression data in islets of obese mice; R.D. performed the bioinformatics analysis; N.K., F.v.M., F.N.V. and K.H. helped with some of the *in vivo* experiments and immunohistochemistry; D.B., J.K.-C. and F.P. obtained human islets and performed quality controls; T.R. performed pronuclei and blastocyst injections; M.S. analyzed and interpreted data, supervised the project and wrote the manuscript.

COMPETING FINANCIAL INTERESTS

The authors declare competing financial interests: details are available in the online version of the paper.

1. Butler, A.E. *et al.* Beta-cell deficit and increased beta-cell apoptosis in humans with type 2 diabetes. *Diabetes* **52**, 102–110 (2003).
2. Song, B., Scheuner, D., Ron, D., Pennathur, S. & Kaufman, R.J. Chop deletion reduces oxidative stress, improves beta cell function, and promotes cell survival in multiple mouse models of diabetes. *J. Clin. Invest.* **118**, 3378–3389 (2008).
3. Barlow, A.D., Nicholson, M.L. & Herbert, T.P. Evidence for rapamycin toxicity in pancreatic beta-cells and a review of the underlying molecular mechanisms. *Diabetes* **62**, 2674–2682 (2013).
4. Robertson, R.P., Harmon, J., Tran, P.O. & Poitout, V. Beta-cell glucose toxicity, lipotoxicity, and chronic oxidative stress in type 2 diabetes. *Diabetes* **53** (suppl. 1), S119–S124 (2004).
5. Volchuk, A. & Ron, D. The endoplasmic reticulum stress response in the pancreatic beta-cell. *Diabetes Obes. Metab.* **12** (suppl. 2), 48–57 (2010).
6. Halban, P.A. *et al.* Beta-cell failure in type 2 diabetes: postulated mechanisms and prospects for prevention and treatment. *Diabetes Care* **37**, 1751–1758 (2014).
7. Friedman, R.C., Farh, K.K., Burge, C.B. & Bartel, D.P. Most mammalian mRNAs are conserved targets of microRNAs. *Genome Res.* **19**, 92–105 (2009).
8. Bartel, D.P. MicroRNAs: target recognition and regulatory functions. *Cell* **136**, 215–233 (2009).
9. Poy, M.N. *et al.* A pancreatic islet-specific microRNA regulates insulin secretion. *Nature* **432**, 226–230 (2004).
10. Latreille, M. *et al.* MicroRNA-7a regulates pancreatic beta cell function. *J. Clin. Invest.* **124**, 2722–2735 (2014).
11. Kameswaran, V. *et al.* Epigenetic regulation of the DLK1–MEG3 microRNA cluster in human type 2 diabetic islets. *Cell Metab.* **19**, 135–145 (2014).
12. Xu, G., Chen, J., Jing, G. & Shalev, A. Thioredoxin-interacting protein regulates insulin transcription through microRNA-204. *Nat. Med.* **19**, 1141–1146 (2013).
13. Kornfeld, J.W. *et al.* Obesity-induced overexpression of miR-802 impairs glucose metabolism through silencing of Hnf1b. *Nature* **494**, 111–115 (2013).
14. Vidigal, J.A. & Ventura, A. The biological functions of miRNAs: lessons from *in vivo* studies. *Trends Cell Biol.* **25**, 137–147 (2015).
15. Trajkovski, M., Ahmed, K., Esau, C.C. & Stoffel, M. MyomiR-133 regulates brown fat differentiation through Prdm16. *Nat. Cell Biol.* **14**, 1330–1335 (2012).
16. Park, S.M., Gaur, A.B., Lengyel, E. & Peter, M.E. The miR-200 family determines the epithelial phenotype of cancer cells by targeting the E-cadherin repressors ZEB1 and ZEB2. *Genes Dev.* **22**, 894–907 (2008).
17. Kim, Y.K. *et al.* TALEN-based knockout library for human microRNAs. *Nat. Struct. Mol. Biol.* **20**, 1458–1464 (2013).
18. Burk, U. *et al.* A reciprocal repression between ZEB1 and members of the miR-200 family promotes EMT and invasion in cancer cells. *EMBO Rep.* **9**, 582–589 (2008).
19. Song, S.J. *et al.* MicroRNA-antagonism regulates breast cancer stemness and metastasis via TET-family-dependent chromatin remodeling. *Cell* **154**, 311–324 (2013).
20. Korpal, M. *et al.* Direct targeting of Sec23a by miR-200s influences cancer cell secretome and promotes metastatic colonization. *Nat. Med.* **17**, 1101–1108 (2011).
21. Hasuwa, H., Ueda, J., Ikawa, M. & Okabe, M. miR-200b and miR-429 function in mouse ovulation and are essential for female fertility. *Science* **341**, 71–73 (2013).
22. Klein, D. *et al.* MicroRNA expression in alpha and beta cells of human pancreatic islets. *PLoS ONE* **8**, e55064 (2013).
23. Filios, S.R. *et al.* MicroRNA-200 is induced by thioredoxin-interacting protein and regulates zeb1 protein signaling and beta cell apoptosis. *J. Biol. Chem.* **289**, 36275–36283 (2014).
24. Pullen, T.J., da Silva Xavier, G., Kelsey, G. & Rutter, G.A. miR-29a and miR-29b contribute to pancreatic beta-cell-specific silencing of monocarboxylate transporter 1 (Mct1). *Mol. Cell. Biol.* **31**, 3182–3194 (2011).
25. Puff, R. *et al.* Reduced proliferation and a high apoptotic frequency of pancreatic beta cells contribute to genetically-determined diabetes susceptibility of db/db BKS mice. *Horm. Metab. Res.* **43**, 306–311 (2011).
26. Ardestani, A. *et al.* MST1 is a key regulator of beta cell apoptosis and dysfunction in diabetes. *Nat. Med.* **20**, 385–397 (2014).
27. Talchai, C., Xuan, S., Lin, H.V., Sussel, L. & Accili, D. Pancreatic beta cell dedifferentiation as a mechanism of diabetic beta cell failure. *Cell* **150**, 1223–1234 (2012).
28. Mandelbaum, A.D. *et al.* Dysregulation of Dicer1 in beta cells impairs islet architecture and glucose metabolism. *Exp. Diabetes Res.* **2012**, 470302 (2012).
29. Leung, A.K. & Sharp, P.A. microRNAs: a safeguard against turmoil? *Cell* **130**, 581–585 (2007).
30. Tornovsky-Babeay, S. *et al.* Type 2 diabetes and congenital hyperinsulinism cause DNA double-strand breaks and p53 activity in beta cells. *Cell Metab.* **19**, 109–121 (2014).
31. Tonne, J.M. *et al.* Global gene expression profiling of pancreatic islets in mice during streptozotocin-induced beta-cell damage and pancreatic Glp-1 gene therapy. *Dis. Model. Mech.* **6**, 1236–1245 (2013).
32. Eichhorn, S.W. *et al.* mRNA destabilization is the dominant effect of mammalian microRNAs by the time substantial repression ensues. *Mol. Cell* **56**, 104–115 (2014).
33. Ladiges, W.C. *et al.* Pancreatic beta-cell failure and diabetes in mice with a deletion mutation of the endoplasmic reticulum molecular chaperone gene P58IPK. *Diabetes* **54**, 1074–1081 (2005).
34. Zeggini, E. *et al.* Meta-analysis of genome-wide association data and large-scale replication identifies additional susceptibility loci for type 2 diabetes. *Nat. Genet.* **40**, 638–645 (2008).
35. Marselli, L. *et al.* Gene expression profiles of Beta-cell enriched tissue obtained by laser capture microdissection from subjects with type 2 diabetes. *PLoS ONE* **5**, e11499 (2010).
36. Harada, H., Andersen, J.S., Mann, M., Terada, N. & Korsmeyer, S.J. p70S6 kinase signals cell survival as well as growth, inactivating the pro-apoptotic molecule BAD. *Proc. Natl. Acad. Sci. USA* **98**, 9666–9670 (2001).
37. Danial, N.N. *et al.* Dual role of proapoptotic BAD in insulin secretion and beta cell survival. *Nat. Med.* **14**, 144–153 (2008).
38. Emamaullee, J.A. *et al.* XIAP overexpression in human islets prevents early posttransplant apoptosis and reduces the islet mass needed to treat diabetes. *Diabetes* **54**, 2541–2548 (2005).
39. Plesner, A., Liston, P., Tan, R., Korneluk, R.G. & Verchere, C.B. The X-linked inhibitor of apoptosis protein enhances survival of murine islet allografts. *Diabetes* **54**, 2533–2540 (2005).
40. Harlin, H., Reffey, S.B., Duckett, C.S., Lindsten, T. & Thompson, C.B. Characterization of XIAP-deficient mice. *Mol. Cell. Biol.* **21**, 3604–3608 (2001).
41. Yan, W. *et al.* Control of PERK eIF2alpha kinase activity by the endoplasmic reticulum stress-induced molecular chaperone P58IPK. *Proc. Natl. Acad. Sci. USA* **99**, 15920–15925 (2002).
42. Shang, X. *et al.* Dual-specificity phosphatase 26 is a novel p53 phosphatase and inhibits p53 tumor suppressor functions in human neuroblastoma. *Oncogene* **29**, 4938–4946 (2010).
43. Armata, H.L., Garlick, D.S. & Sluss, H.K. The ataxia telangiectasia-mutated target site Ser18 is required for p53-mediated tumor suppression. *Cancer Res.* **67**, 11696–11703 (2007).
44. Couch, F.J. *et al.* Association of mitotic regulation pathway polymorphisms with pancreatic cancer risk and outcome. *Cancer Epidemiol. Biomarkers Prev.* **19**, 251–257 (2010).
45. Cunha, D.A. *et al.* Death protein 5 and p53-upregulated modulator of apoptosis mediate the endoplasmic reticulum stress-mitochondrial dialog triggering lipotoxic rodent and human beta-cell apoptosis. *Diabetes* **61**, 2763–2775 (2012).
46. McKenzie, M.D. *et al.* Glucose induces pancreatic islet cell apoptosis that requires the BH3-only proteins Bim and Puma and multi-BH domain protein Bax. *Diabetes* **59**, 644–652 (2010).
47. Hartman, M.G. *et al.* Role for activating transcription factor 3 in stress-induced beta-cell apoptosis. *Mol. Cell. Biol.* **24**, 5721–5732 (2004).
48. Kawase, T. *et al.* PH domain-only protein PHLDA3 is a p53-regulated repressor of Akt. *Cell* **136**, 535–550 (2009).
49. Hashimoto, N. *et al.* Ablation of PDK1 in pancreatic beta cells induces diabetes as a result of loss of beta cell mass. *Nat. Genet.* **38**, 589–593 (2006).
50. Hanahan, D. Heritable formation of pancreatic beta-cell tumours in transgenic mice expressing recombinant insulin/simian virus 40 oncogenes. *Nature* **315**, 115–122 (1985).
51. Chipuk, J.E. *et al.* Direct activation of Bax by p53 mediates mitochondrial membrane permeabilization and apoptosis. *Science* **303**, 1010–1014 (2004).
52. Krützfeldt, J. *et al.* Silencing of microRNAs *in vivo* with 'antagomirs'. *Nature* **438**, 685–689 (2005).
53. Obad, S. *et al.* Silencing of microRNA families by seed-targeting tiny LNAs. *Nat. Genet.* **43**, 371–378 (2011).
54. Chang, C.J. *et al.* p53 regulates epithelial-mesenchymal transition and stem cell properties through modulating miRNAs. *Nat. Cell Biol.* **13**, 317–323 (2011).
55. Jiang, H.Y. *et al.* Activating transcription factor 3 is integral to the eukaryotic initiation factor 2 kinase stress response. *Mol. Cell. Biol.* **24**, 1365–1377 (2004).
56. Zmuda, E.J. *et al.* Deficiency of Atf3, an adaptive-response gene, protects islets and ameliorates inflammation in a syngeneic mouse transplantation model. *Diabetologia* **53**, 1438–1450 (2010).
57. Thomas, G. *et al.* Multiple loci identified in a genome-wide association study of prostate cancer. *Nat. Genet.* **40**, 310–315 (2008).
58. Ohki, R. *et al.* PHLDA3 is a novel tumor suppressor of pancreatic neuroendocrine tumors. *Proc. Natl. Acad. Sci. USA* **111**, E2404–E2413 (2014).

ONLINE METHODS

Experimental animals. All animal models were on a C57BL/6N background. For *db/db* mice the respective WT mice were on a BLKS background. For breedings, C57BL/6N male and female mice were purchased from either Janvier or Harlan. Mice were housed in a pathogen-free animal facility at the Institute of Molecular Systems Biology at the ETH Zurich. The animals were maintained in a temperature-controlled room (22 °C), with humidity at 55% and on a 12 h light-dark cycle (lights on from 6 a.m. to 6 p.m.). Mice were fed a standard laboratory chow or a HFD (fat, carbohydrate, protein content was 45, 35 and 20 kcal%, respectively) (Research Diets, D12451), and water *ad libitum*, and the age of mice is either indicated in the Figures or was above 8 weeks of age. Male mice were used for all studies shown. All animal experiments were approved by the Kantonale Veterinäramt Zürich. Generation of mice deficient for *mir-141/200c* and *mir-200a, mir-200b, mir-429* was performed in C57BL/6N embryonic stem (B6 ES) cells and breeding schemes are described below. *Bad*$^{-/-}$, *Rip-Tag2*, and *Trp53*$^{-/-}$ mice have been published previously[50,59,60]. *Rip*-Cre mice were kindly provided by P. Herrera. Akita and *Bax*$^{-/-}$ mice were purchased from Jackson Laboratories.

Blood glucose measurements and intraperitoneal glucose tolerance tests. Blood glucose was measured using a Contour glucometer (Bayer). For intraperitoneal glucose tolerance tests, mice were fasted for 4 h and then by injected with of 2 g/kg body weight D-glucose in PBS.

Insulin measurements. For measuring mouse serum insulin levels, blood was collected from the tail vein, the serum was separated by centrifugation and insulin was measured by ELISA (Chrystal Chem). For determining total pancreatic insulin contents, hormones were extracted by acid-ethanol extraction and concentrations were determined by ELISA.

Antibodies. The following antibodies were used in immunohistochemistry or immunoblotting: anti-insulin (DAKO, #A0564, 1:1,000), anti-glucagon (Millipore, #AB932, 1:200), anti-Ki-67 (BD Bioscience, #556003, 1:100), anti-phospho-histone H2A.X (Ser139) (Cell Signaling, #2577S, 1:100), anti-phospho-p53 (Ser15) (Cell Signaling, #12571S, 1:1,000), anti-p53 (Cell Signaling, #2524S, 1:1,000), guinea pig anti-insulin (Invitrogen, #18-0067, 1:1,000), mouse anti-Ki-67 (BD Biosciences, #556003, 1:100), rabbit anti-pS139-H2A.X (Cell Signaling, #2577, 1:100), mouse anti-γ-tubulin (Sigma, #T6557, 1:2000), rabbit anti-beta-actin (Cell Signaling, #4970, 1:2,000–5,000), rabbit anti-cleaved caspase 3 (Cell Signaling, #9661, 1:500), mouse anti-caspase 9 (Cell Signaling, #9508, 1:1,000), rabbit anti-PCNA (Cell Signaling, #2586, 1:1,000), rabbit anti-p-eiF2a (Cell Signaling, #3398, 1:1,000) and rabbit anti-eiF2a (Cell Signaling, #5324, 1:1,000).

Immunohistochemistry and islet morphometry. Pancreata were fixed in 4% paraformaldehyde (PFA) and embedded in paraffin, and the cut sections were antigen retrieved by boiling them in 10 mM Tris/EDTA (pH 9.0). The sections were permeabilized and blocked in PBS containing 0.1% Triton X-100, 1% BSA and 5% donkey or goat serum. Primary antibody binding was performed overnight at 4 °C, while secondary antibody incubation was carried out at room temperature (21 °C) for 1 h. For pancreas morphometry analysis, 8 µm sections were cut and 3–5 sections that were at least 180 µm apart were taken from each mouse for each type of analysis. For determining beta cell and alpha cell mass, the sections were stained with anti-insulin and anti-glucagon antibodies and DAPI. The pancreatic sections were scanned entirely using a 10× objective of a Zeiss AxioVert 200 microscope or a 20× objective of the Pannoramic 250 Slide scanner (3D Histech). The fraction of the insulin- or glucagon-positive areas compared to total (DAPI-stained) area was determined using NIH ImageJ software (http://rsbweb.nih.gov/ij/download) and the mass was calculated by multiplying this fraction by the initial pancreatic wet weight.

Immunohistochemistry of lymphocyte markers. Stainings were performed on 3 µm sections from 6-week-old *Rip141/200c* and WT (Ctrl) mice. All incubations were performed on a Bond III system (Leica). The detection was done using the Refine DAB Kit (Refine Rb-a-Rat IgG HRP for PTPRC (B220) and ADGRE1; Refine RbAk-on-Ms HRP for CD3) and pretreatment was performed using enzyme 1 for ADGRE1 and pretreatment buffer 2 for CD3 and PTPRC (all reagents from Leica). Sections were evaluated on a Zeiss AxioImager A1.

Lineage-tracing studies. *Rip*-Cre mice were crossed into *Rosa26-tdRFP* mice, which inherit a RFP reporter gene preceded by a floxed Stop cassette in the Rosa locus. Upon Cre expression the Stop cassette will be excised and RFP will be expressed. The offspring containing both mutant alleles was further bred with *Rip141/200c* mice to obtain triple mutant mice. Mice were killed at the age of 17 weeks, pancreata were taken and fixed in 4% PFA for 2 h at 21 °C before being cryo-embedded (OCT-Tissue fixative). Sections of 10 µm were stained for glucagon, mounted with DAPI and sealed. Images were taken at a Zeiss confocal microscope.

RNA isolation and quantification. RNA was isolated using TRIzol reagent (Invitrogen) according to the manufacturer's protocol. RNA was subjected to DNase I treatment with the DNA-free kit (Invitrogen), when necessary. RNA was reverse transcribed using High Capacity cDNA Reverse Transcription Kit (Applied Biosystems). Quantitative PCR was performed in an LC480 II Lightcycler (Roche) and using gene specific primers and either Light Cycler 480 SYBR Green Master mix (Roche) or Sybr Fast 2x Universal Master mix (Kapa). Results were normalized to 36B4 or Cyclophilin E mRNA levels. microRNA levels were measured using the TaqMan microRNA assays (Applied Biosystems) and the results were normalized to miR-16 or sno-202 levels. For absolute quantification, mature full-length miRs were synthesized (Sigma).

Generation of *Rip141/200c* transgenic mice. Transgenic mice expressing *mir-141/200c* under the regulation of the rat insulin promoter (Rip) was created by subcloning the rat insulin II promoter in pCRII (Invitrogen) by TOPO cloning. An 819 bp fragment containing the genomic mouse *pri-mir-141/200c* sequence was inserted downstream of the Rip and a 1.8 kb XhoI/*Spe1* fragment was microinjected into male pronuclei of C57BL/6N zygotes to generate *Rip141/200c* transgenic animals. Three transgenic (E4, E44, E46) founder lines were characterized. All lines displayed similar expression levels of miR-141 and miR-200c (4–6-fold overexpression) and a profoundly diabetic phenotype. Data presented here were obtained with E4. All mice were maintained on a pure C57BL/6N background. Genotyping of transgenic mice was performed by Southern blotting (**Supplementary Fig. 1**) or PCR using primers listed in **Supplementary Table 2**.

Islet secretion studies. Islet secretion studies were performed on size-matched islets isolated from 2-week-old animals following collagenase digestion and overnight culture. We used Dulbecco's PBS-HEPES-BSA buffer at 3.3 mM and 10 mM glucose and, after an equilibration period of 15 min, we continuously perfused islets with each concentration for 5 min and collected the flowthrough at a rate of 100 µl/min (National Instruments, Bioprep Technology). Values are normalized to total insulin content.

Cell culture, transfection and viral infections. MIN6 cells were maintained in DMEM medium as described previously[9]. INS-1E cells were cultivated in RPMI 1640 with 10% FCS, 2 mM Glutamax, 10 mM HEPES, 5 µM beta-mercaptoethanol and 100 U/ml penicillin/streptomycin. HEK 293 cells were grown in DMEM media containing 4.5 g/l glucose, 10% FBS and 100 U/ml penicillin/streptomycin under 5% CO_2 atmosphere at 37 °C. All cell lines were tested for glucose-stimulated insulin secretion and mycoplasma upon acquisition and routinely every 6 months, but were not authenticated by STR profiling. All transfections were performed using Lipofectamine 2000 or Lipofectamine RNAiMAX (both from Life Technologies), according to the product manual. siRNAs (Sigma-Aldrich or Microsynth), miR mimics (Dharmacon or Microsynth) and LNAs (Exiqon) were transfected at 40–100 nM. Cells were harvested 48–72 h after transfection. MIN6 and INS-1E adenoviral infections were performed at a multiplicity of infection of 25 for 36–48 h in normal medium, which was exchanged after 24 h.

Plasmids and recombinant adenoviruses. Mouse miR-141/200c–expressing vectors were generated by PCR amplification of 450 bp– and 250 bp–spanning genomic sequences of *pre-mir-141/200c*. Fragments were cloned at XhoI sites of pcDNA3 and pAD5 for adenovirus production (Viraquest). All adenoviruses

doi:10.1038/nm.3862

expressed GFP from an independent (RSV) promoter. Mouse 3′ UTR sequences of putative miR-200 target genes were PCR-amplified from mouse DNA or synthesized (Genescript) and cloned into pmirGLO. Mutagenesis of the miR-200 seed motifs in the 3′ UTR of selected targets was performed using QuikChange Lightning kit (Agilent Technologies) or by *de novo* DNA synthesis (Genescript). All constructs and derived mutants were confirmed by DNA sequencing.

Immunoblotting. Supernatants (containing dead/dying cells) and trypsinized cells were spun down for 5 min at 100 *g*, and the resulting cell pellet was lysed in PBS containing 150 mM NaCl and 1% Triton X-100 supplemented with cOmplete EDTA-free protease inhibitors (Roche) and Halt Phosphatase inhibitors (Pierce). Protein concentrations were measured by Bicinchonic Acid (BCA) method. Laemmli buffer was added to samples, equal protein amounts were separated by SDS–PAGE, transferred by electroblotting and membranes were blocked in 5% milk/TBS-T or 5% BSA/TBS-T for 1 h. Membranes were incubated with appropriate antibodies overnight at 4 °C. Membranes were exposed to secondary antibodies for 1 h at room temperature and developed using ECL Western Blotting Substrate (Pierce).

Automated cell counts. For automated cell counts, 15,000 MIN6 or 10,000 INS-1E cells were split onto 96-well plates with glass bottoms (Greiner). Only the inner 32 (8 × 4) wells were used for analysis to prevent edge effects. 48–72 h after transfection, 150 µl of 8% PFA containing Hoechst 33342 (1 µg/ml) was added to the medium of each well, and plates were incubated on a shaker for 15 min at room temperature. Medium/PFA was discarded, and all wells were washed 3× with PBS. 3 × 3 pictures were taken from each well with an ImageXpress Micro automated microscope at 10× magnification (Molecular Devices). Hoechst-stained nuclei were detected by Cellprofiler Software. All pipetting steps were performed with calibrated multi-channel pipettes (Eppendorf). A maximum of eight conditions (in quadruplicates) were assayed on any given plate, with the respective control (si-Ctrl pool, miR-Ctrl or CMV-mCherry) always present for normalization and statistical analysis.

Generation of *mir-141/200c*$^{-/-}$ mice. The cloning of the *mir-141/200c* genomic sequences was achieved from a C57BL/6 library and a ~40 kb fragment encoding *mir-141/200c* was subcloned. This clone was used to PCR amplify a 2 kb fragment as the 5′ arm and to isolate a 4.6 kb EcoRI/*Nhe*I fragment as the 3′ arm. Genomic sequences were cloned into pPNT2L3 vector containing resistance cassettes for positive and negative selection. The construct was linearized and electroporated into C57BL/6J ES cells. Twelve days after electroporation and selection in hygromycin-containing medium, colonies were isolated and analyzed by Southern blotting. We observed a homologous recombination frequency of ~5%. Three ES cell clones with the confirmed targeted mutation were injected into BALB/c blastocysts (3.5 d) and these were subsequently transferred into CD1- and B6D2F1-surrogate mothers. The resulting male chimeras were mated to C57BL/6N females and offspring from germline transmission, scored by coat color, were analyzed. The transmission of the targeted *mir-141/200c* gene was demonstrated by Southern blotting of tail DNA and heterozygote C57BL/6N *miR141/200c*^{tm1Biat} mutants were further mated to B6N WT mice.

Generation of mir-200a–, mir-200b– and mir-429–deficient mice. To generate the targeting construct, a DNA fragment containing the mouse *mir-200a/200b/429* locus was subcloned from bacterial artificial chromosome (BAC RP24-325H12) using the Red/ET cloning technique according to the protocol by Gene Bridges (http://www.genebridges.com). Lox*P* sites were introduced 5′ and 3′ in close proximity to the *mir-200* locus together with a neomycin-resistance cassette flanked by *Frt* sites (**Supplementary Fig. 3a**). Upon linearization, the targeting vector was electroporated into embryonic stem cells derived from C57BL/6N mice, and then ES cell clones were selected with G418 (Invitrogen) and verified by Southern blotting. Correctly targeted clones were injected into BALB/c blastocysts and transferred into pseudopregnant females to generate chimeric offspring. Chimeras were bred with C57BL/6 mice to generate heterozygous progeny and germline transmission of the mutated allele was verified by PCR. The neomycin cassette was excised by intercrossing with transgenic deleter-Flippase mice, leaving the floxed *mir-200* locus and a lone *Frt* site. These mice were intercrossed with Rip-Cre mice to obtain mice lacking *mir-200* in pancreatic beta cells. Genotyping of *miR-200*–floxed mice was performed by PCR on genomic DNA using primers listed in a **Supplementary Table 2**.

Southern blotting. Genomic DNA isolated from mouse tail biopsies was digested overnight with restriction enzymes at 37 °C, loaded on 0.8% Tris-Acetate-EDTA agarose gels and transferred to nylon blotting membrane (Bio-Rad). Membranes were UV-cross-linked and incubated at 85 °C for 1 h. Probes were PCR amplified from genomic DNA using primers listed in **Supplementary Table 2**, radiolabeled with ^{32}P using the Prime-It Random Primer Labeling kit (Agilent Technologies) and purified by G50 gel filtration (GE Healthcare). Membranes were hybridized with probes overnight at 62 °C, washed and exposed to x-ray films.

Multiple low-dose STZ treatment *in vivo*. Doses of 40 mg/kg streptozotocin (Sigma, S0130-1G) were injected daily for 5 d. Before injection with STZ, mice were fasted for 4 h and STZ was freshly dissolved in sodium citrate buffer (0.1 M, pH 4.5) immediately before the experiment.

HFD and single high-dose STZ treatment. Male mice were fed a HFD (Research Diets, New Brunswick, NJ) starting at 4 weeks of age and body weight and blood glucose levels were recorded weekly for 8 weeks. Mice were then subjected to intraperitoneal insulin tolerance tests (0.75 U/kg). On the following day, mice were fasted for 6 h and injected with a single dose of STZ at 150 mg/kg (freshly dissolved in 0.1 M sodium citrate buffer, pH 4.5). Blood glucose levels were measured for 4 d and mice were then killed for immunohistological analysis of beta cell mass.

Luciferase assays. MIN6 or HEK 293 cells were cultured in 24-well plates and transfected with 100 ng pmirGLO reporters in combination with miR mimics (50 nM). Cells were harvested and assayed 48 h after transfection using the Dual-Luciferase Reporter Assay System (Promega). Results were normalized to the Renilla luciferase control contained in pmirGLO and expressed relative to the average value of the controls.

Affymetrix gene-expression analysis. The expression analysis of total RNA extracted from islets of 6-week-old *Rip141/200c* mice using TRIzol reagent (Invitrogen) was performed using Affymetrix mouse genome 430 2.0 array. Analysis of total RNA extracted from MIN6 cells infected with recombinant adenovirus expressing miR-141/200c was performed using the Affymetrix mouse genome 430A 2.0 array.

Illumina RNA sequencing. *Library preparation.* The quality of the isolated RNA was determined with a Qubit (1.0) Fluorometer (Life Technologies, California, USA) and a Bioanalyzer 2100 (Agilent, Waldbronn, Germany). Only those samples with a 260/280 nm ratio between 1.8 and 2.1 and a 28S/18S ratio within 1.5 and 2.0 were further processed. The TruSeq RNA Sample Prep Kit v2 (Illumina, Inc, California, USA) was used in the succeeding steps. Briefly, total RNA samples (100–1,000 ng) were polyA enriched and then reverse transcribed into double-stranded cDNA. The cDNA samples were fragmented, end repaired and polyadenylated before ligation of TruSeq adaptors containing the index for multiplexing Fragments on both ends were selectively enriched with PCR. The quality and quantity of the enriched libraries were validated using Qubit (1.0) Fluorometer and the Caliper GX LabChip GX (Caliper Life Sciences, Inc., USA). The product is a smear with an average fragment size of approximately 260 bp. The libraries were normalized to 10 nM in Tris-Cl 10 mM, pH 8.5 with 0.1% Tween-20.

Cluster generation and sequencing. The TruSeq PE Cluster Kit v3-cBot-HS or TruSeq SR Cluster Kit v3-cBot-HS (Illumina, Inc, California, USA) was used for cluster generation using 10 pM of pooled normalized libraries on the cBOT. Sequencing was performed on the Illumina HiSeq 2000, paired end at 2 × 101 bp or single end at 100 bp using the TruSeq SBS Kit v3-HS (Illumina, Inc, California, USA).

Data analysis. RNA-seq reads were quality checked with fastqc, which computes various quality metrics for the raw reads. Reads were aligned to the genome and transcriptome with TopHat v. 1.3.3. Before mapping, the low-quality ends of the reads were clipped (three bases from the read start and 10 bases from the

read end). TopHat was run with default options. The 'fragment length' parameter was set to 100 bases with a standard deviation of 100 bases. On the basis of these alignments, the distribution of the reads across genomic features was assessed. Isoform expression was quantified with the RSEM algorithm[61] with the option for estimation of the read start position distribution turned on.

miR expression analysis. 150 ng of total RNA was reverse transcribed using TaqMan MicroRNA Assays (Life Technologies) and TaqMan MicroRNA Reverse Transcription Kit (Life Technologies). The reverse transcription primers were multiplexed in a dilution of 1:20 as described by the manufacturer. Quantitative PCR reactions were performed with the Light Cycler 480 (Roche) employing a 384-well format, TaqMan Universal PCR Master Mix, No AmpErase UNG (Life Technologies) and TaqMan MicroRNA Assays (Life Technologies). Cycles were quantified employing Light Cycler 480 analysis software (Abs quantification/second derivate max). Relative miR expression was calculated using the ddCT method. For absolute quantification, synthetic miRs (Sigma-Aldrich) were quantified using a NanoDrop ND-1000 spectrophotometer (Thermo Scientific) and the respective molecular weight. miRs were absolutely quantified employing a synthetic miR standard curve.

Seed enrichment analysis. Seed enrichment analysis was performed as published recently using Targetscan[62,63].

Human pancreatic islets. Human islets were received from nondiabetic healthy donors. Informed consent was obtained for all subjects. Islets were handpicked and purity was greater than 95%. Human pancreata were harvested from brain-dead organ donors after obtaining informed consent from family members in agreement with the French Regulations and with Lille's Institutional Ethical Committee (Comité d'Ethique du Centre Hospitalier Régional et Universitaire de Lille) and in accordance the Institutional Review Board of the Departments of Neurology, Dermatology, Anesthesiology and Surgery by delegation of the Institutional Review Board of Geneva University Hospitals. The islet preparation of donors (age range, 21–65; 4 males, 3 females) consisted of 15,000–25,000 islet equivalents with a purity of >80%. All preparations had a viability of >90%. All experiments were performed in five to six technical replicates with islets from individual donors. Pancreatic islets were handpicked under a microscope and cultured in CMRL-1066 medium containing 5.6 mM glucose, 10% FBS, 100 IU/ml penicillin/streptomycin and Glutamax. For target gene expression, islets were cultured for 48 h in the presence of anti-miRs or antagomirs at a concentration of 50 μg/ml, followed RNA extraction using TRIzol. For stress-response assays, islets were cultured for 24 h in the presence of anti-miRs or antagomirs at a concentration of 50 μg/ml before cytokine/palmitate treatment (in the presence of anti-miRs) for 24 h. Palmitate-conjugated BSA was used at a 1 mM concentration, the cytokine cocktail consisted of IL-1β (50 U/ml), TNF-α (1,000 U/ml) and IFN-γ (1,000 U/ml).

MicroRNA inhibitors. Optimized single-strand modified RNA analogs used in this study were synthesized by Axolabs (Kulmbach, Germany). The term 'antagomirs' refers to cholesterol-conjugated modified RNAs[52]. The term 'anti-miRs' refers to unconjugated modified RNAs. Oligonucleotides used in this study consisted of either 23 nucleotides (full-length) or 13 nucleotides, covering the seed sequence, with modifications as specified in **Supplementary Table 2**.

Chemicals. Nutlin-3 (ref. 64) (Sigma-Aldrich) was dissolved in pure DMSO at a concentration of 10 mg/ml (1,000× stock). Tunicamycin (Calbiochem) was dissolved in pure DMSO (stock concentration, 5 mg/ml, 2,500× stock). Etoposide was dissolved in pure DMSO (stock concentration, 25 mM, 500× stock). STZ (Sigma-Aldrich) was dissolved in full medium immediately before use *in vitro*. Where applicable, DMSO was used as a control.

Statistical analysis. Numerical values are reported as average ± s.d. unless stated otherwise. Data is derived from multiple independent experiments from distinct mice or cell culture plates, unless stated otherwise. No statistical method was used to predetermine sample size, but sample size was based on preliminary data and previous publications as well as observed effect sizes. Outliers that were two standard deviations outside of the mean were routinely excluded from all analyses. No randomization of animals was performed, but animals were sex- and age-matched, and littermates were used whenever possible. Animal studies were performed without blinding of the investigator. We assessed data for normal distribution and similar variance between groups using GraphPad Prism 6.0 if applicable. Some data sets had a statistical difference in the variation between groups. If not mentioned otherwise in the figure legend, statistical significance ($^{*}P \leq 0.05$, $^{**}P \leq 0.01$, $^{***}P \leq 0.001$) was determined by unpaired two-tailed *t*-test, or one-way ANOVA with relevant *post hoc* tests (Tukey's if not specified otherwise). *P* values and *z*-scores for signaling networks were determined by Ingenuity software (Qiagen). We used GraphPad Prism 6.0 Software for statistical analysis of all other data sets.

59. Ranger, A.M. *et al.* Bad-deficient mice develop diffuse large B cell lymphoma. *Proc. Natl. Acad. Sci. USA* **100**, 9324–9329 (2003).
60. Olive, K.P. *et al.* Mutant p53 gain of function in two mouse models of Li-Fraumeni syndrome. *Cell* **119**, 847–860 (2004).
61. Li, B. & Dewey, C.N. RSEM: accurate transcript quantification from RNA-Seq data with or without a reference genome. *BMC Bioinformatics* **12**, 323 (2011).
62. Denzler, R., Agarwal, V., Stefano, J., Bartel, D.P. & Stoffel, M. Assessing the ceRNA hypothesis with quantitative measurements of miRNA and target abundance. *Mol. Cell* **54**, 766–776 (2014).
63. Friedman, R.C., Farh, K.K.-H., Burge, C.B. & Bartel, D.P. Most mammalian mRNAs are conserved targets of microRNAs. *Genome Res.* **19**, 92–105 (2009).
64. Vassilev, L.T. *et al. In vivo* activation of the p53 pathway by small-molecule antagonists of MDM2. *Science* **303**, 844–848 (2004).

doi:10.1038/nm.3862